THE JOURNAL OF PHYSICAL CHEMISTRY Letters

pubs.acs.org/JPCL

Letter

Ultrafast Charge Dynamics in Dilute-Donor versus Highly Intermixed TAPC:C_{60} Organic Solar Cell Blends

Gareth John Moore, Martina Causa', Josue F. Martinez Hardigree, Safakath Karuthedath, Ivan Ramirez, Anna Jungbluth, Frédéric Laquai, Moritz Riede, and Natalie Banerji*

Cite This: *J. Phys. Chem. Lett.* 2020, 11, 5610–5617

Read Online

ACCESS | Metrics & More | Article Recommendations | Supporting Information

ABSTRACT: Elucidating the interplay between film morphology, photophysics, and device performance of bulk heterojunction (BHJ) organic photovoltaics remains challenging. Here, we use the well-defined morphology of vapor-deposited di-[4-(*N*,*N*-di-*p*-tolyl-amino)-phenyl]-cyclohexane (TAPC):C_{60} blends to address charge generation and recombination by transient ultrafast spectroscopy. We gain relevant new insights to the functioning of dilute-donor (5% TAPC) fullerene-based BHJs compared to molecularly intermixed systems (50% TAPC). First, we show that intermolecular charge-transfer (CT) excitons in the C_{60} clusters of dilute BHJs rapidly localize to Frenkel excitons prior to dissociating at the donor:acceptor interface. Thus, both Frenkel and CT excitons generate photocurrent over the entire fullerene absorption range. Second, we selectively monitor interfacial and bulk C_{60} clusters via their electro-absorption, demonstrating an energetic gradient that assists free charge generation. Third, we identify a fast (<1 ns) recombination channel, whereby free electrons recombine with trapped holes on isolated TAPC molecules. This can harm the performance of dilute solar cells, unless the electrons are rapidly extracted in efficient devices.

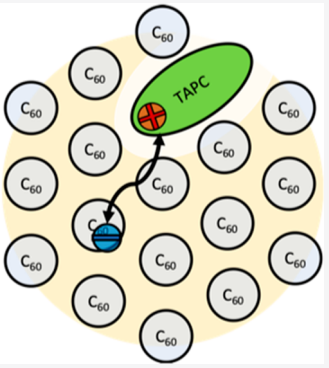

Power conversion efficiencies (PCEs) of up to 18% in organic photovoltaics (OPVs) have renewed the interest in the field and opened further avenues toward large-scale commercialization.[1−5] Nevertheless, many fundamentals of photon-to-current conversion still lack a comprehensive understanding of the underlying mechanisms, mainly because of the energetic and morphological complexity of the photovoltaic active layers. In this respect, all-small-molecule thermally evaporated organic solar cells containing predominantly a fullerene acceptor (>90%) blended with a low amount of donor, so-called "dilute-donor organic solar cells", not only show surprisingly high performance (over 8% PCE)[6,7] but also represent exceptional model systems, where the impact of morphology can largely be decoupled from other parameters under study. In particular, at low donor content, homogeneous dispersion is possible, ensuring that each donor molecule is surrounded by fullerenes, establishing a well-defined donor−acceptor interface.[8,9] Such dilute systems have been used to investigate the molecular parameters determining the energy of interfacial CT states,[10,11] the properties of such CT states,[12−14] the impact of CT-state energetics on charge recombination and open circuit voltage (V_{OC}),[8,14−16] and the hole transport between isolated donor molecules lacking percolation pathways.[17−21]

Here, we comprehensively investigate the subnanosecond charge generation and recombination dynamics of dilute-donor model systems and compare them to the behavior of a molecularly intermixed BHJ. We select TAPC:C_{60} blends (Figure S1), because they show similar interfacial CT-state energy of 1.4−1.5 eV and negligible donor aggregation over a wide range of compositions (5−50% TAPC by weight),[9,14,20] good solar cell performance, and high V_{OC} at dilute donor concentrations.[8] The morphology of the 5% BHJ consists of large C_{60} domains (with coherence lengths of ∼65 Å according to our GIWAXS data, Figure S2) with TAPC molecules isolated and dispersed throughout the blend. The 50% BHJ is notably without large C_{60} domains (∼12 Å coherence length) and presents a highly intermixed donor:acceptor morphology (Figure 1A).[20,22] Thus, we can tune the C_{60} domain size from the low-donor (5% TAPC) to the completely intermixed (50% TAPC) regime, while maintaining constant interfacial energetics. Relevant to both dilute and standard solar cell systems, we gain valuable insights into the effect of excitation energy on exciton dissociation and the local energetic landscape near the interface, and we identify different recombination mechanisms.

All transient absorption (TA) data were recorded with selective excitation of the C_{60} acceptor (which has a distinct absorption from TAPC) and at a low excitation density of $<10^{18}$ cm^{-3}, so that many-body carrier interactions can be

Received: May 14, 2020
Accepted: June 22, 2020
Published: June 22, 2020

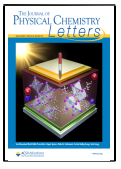

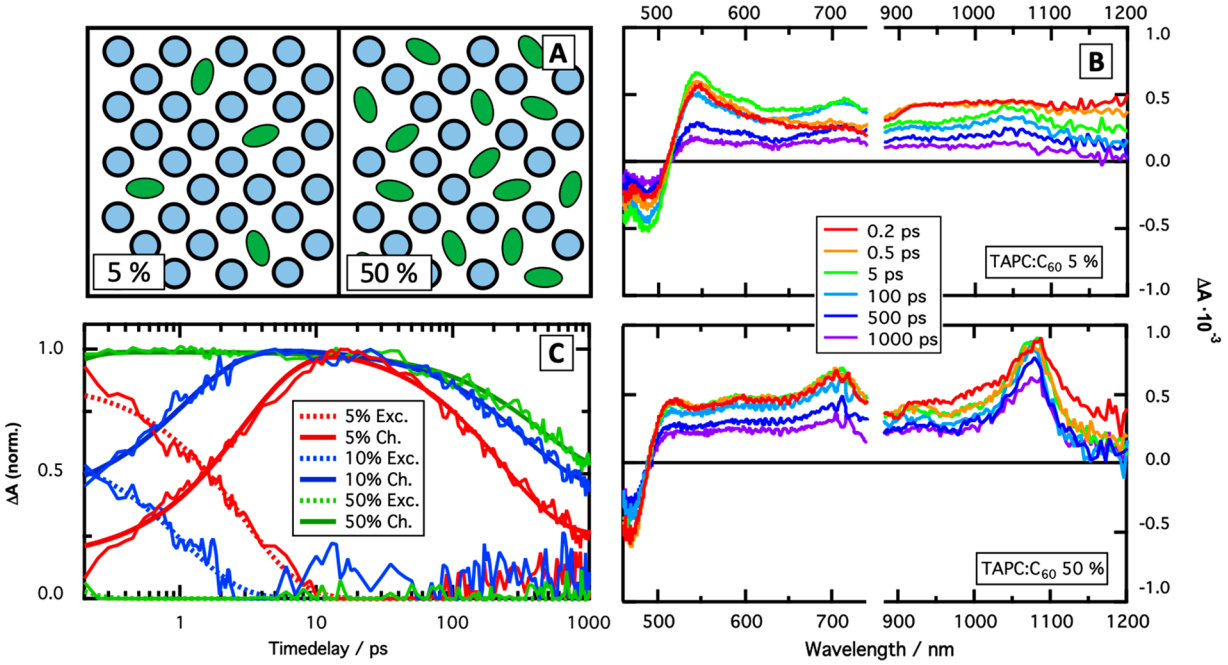

Figure 1. (A) 2D representation of the expected morphology inside the bulk-heterojunctions, with C_{60} represented as blue circles and TAPC as green ellipsoids in 5% and 50% TAPC:C_{60} blends (by weight). (B) Transient absorption (TA) spectra of TAPC:C_{60} blends with a weight ratio of 5% and 50% at selected time delays (0.2 ps, 0.5 ps, 5 ps, 100 ps, 500 ps, and 1 ns) at 610 nm pump excitation. The MCR-ALS decomposition into the dynamics of Frenkel exciton and charge signatures is shown in (C) for 5% (red), 10% (blue), and 50% (green) blends, with a kinetic model analysis of both, excitons (dashed lines) and charges (solid lines).

neglected on the investigated time scale, as evidenced by the fluence-independent dynamics (Figure S3). We have previously shown for neat C_{60} films that excitation at 610 nm yields Frenkel excitons localized on a single C_{60} molecule, while excitation at 450 nm yields inter-C_{60} CT excitons delocalized over several fullerenes (not to be confused with interfacial CT states in donor:acceptor blends).[23] Figure 1B shows the TA spectra of TAPC:C_{60} blends containing 5% (top) and 50% (bottom) donor with 610 nm excitation. At early times (<1 ps), the features of the 5% TA spectrum are dominated by C_{60} Frenkel exciton signatures at 920 and 450 nm, similar to neat C_{60} films (Figure S4).[23] At later times (>5 ps), following diffusion-limited hole transfer (HT) from the C_{60} Frenkel excitons to TAPC, we observe a rise of charge-induced signatures at ∼700 nm for $TAPC^{\bullet+}$ and ∼1055 nm for $C_{60}^{\bullet-}$ and of the oscillatory electro-absorption (EA) peaking at 485 and 545 nm, which is caused by a field-induced shift in the inter-C_{60} CT transitions of large C_{60} clusters (see discussion below). In the TA spectra of the 50% blend, we see prompt charge signatures, because unlike in dilute blends, the molecularly mixed morphology does not require exciton diffusion before HT to TAPC. The anion peak (∼1070 nm) is notably sharper and more pronounced than in the 5% blend, because the anion is localized on isolated C_{60} molecules,[23,24] while its red-shift is likely associated with a change in the environment.[25−27] In the 50% BHJ, the ground-state bleaching (GSB) dominates the negative band at 450 nm, with the EA having a smaller amplitude compared to the 5% blend, which we assign to the absence of large C_{60} clusters (see less pronounced inter-C_{60} CT absorption, Figure S5).

The dynamics of excitons and charges, obtained from the decomposition of the TA spectra into the two corresponding spectral components using multivariate curve resolution with alternating least-squares (MCR-ALS),[28−31] are shown for 5%, 10%, and 50% blends in Figure 1C. These dynamics were subsequently analyzed with a kinetic model (Figure S6), which includes HT from the C_{60} Frenkel excitons to TAPC in competition with their intrinsic decay to the ground state (fixed to 150 ps),[23] and the recombination of part of the charges within the <1 ns time window of the experiment (discussed at the end of the Letter). The time constant for HT follows the trend expected from the morphology and exciton diffusion distance, with HT times decreasing from 3 ps (5% blend) to 1 ps (10% blend) to <100 fs (50% blend), as the availability of TAPC molecules increases and the size of the C_{60} clusters decreases (Table 1 and Figure 1A). Therefore, the fraction of charges generated by prompt HT within the 0.2 ps time resolution of our analysis increases from 20% to 97% when going from the 5% to the 50% blend.

Table 1. Outcome of the Kinetic Modelling of the MCR-ALS Decomposition Dynamics from the TA Data for All Three TAPC:C_{60} Blends (5%, 10%, and 50%)[a]

	5% blend	10% blend	50% blend
C_{init}	20%	50%	97%
$\tau_{exciton}$ (ps)	150 (2%)	150 (1%)	150 (0%)
τ_{HT} (ps)	2.9 (98%)	1.1 (99%)	<0.1 (100%)
τ_{rec} (ps)	280 (75%)	280 (53%)	280 (42%)
C_{long}	25%	47%	58%

[a]Initial charge population at 0.2 ps (C_{init}) expressed as a fraction of the total excitation density, intrinsic exciton lifetime ($\tau_{exciton}$) and fraction of excitons decaying to the ground state, hole-transfer time constant (τ_{HT}) and fraction of excitons undergoing hole transfer, charge recombination time constant (τ_{rec}) and fraction of charges undergoing recombination, and offset due to long-lived charges (C_{long}) expressed as a fraction of the total charge population.

https://dx.doi.org/10.1021/acs.jpclett.0c01495
J. Phys. Chem. Lett. 2020, 11, 5610−5617

In neat C_{60} films, excitation at 450 nm yields delocalized inter-C_{60} CT excitons, characterized by a pronounced EA signature peaking at 550 nm and relaxing to Frenkel excitons within 0.2 ps.[23,32] Inter-C_{60} CT excitons can also be generated in the fullerene clusters of dilute-donor BHJs. To evaluate their impact on the HT mechanism to donor molecules, we have measured the TA spectra of the 5% TAPC:C_{60} film excited at 450 nm, and we compare the dynamics probed at 550 nm (overlap of EA, exciton and charge signatures) to 610 nm excitation in Figure 2A. There is a notable decay in the signal with 450 nm excitation on the 1 ps time scale, after which, the rise corresponding to HT and subsequent decay due to charge recombination are the same at both excitation wavelengths. Figure 2B shows the MCR-ALS decomposition dynamics obtained from the TA data at 450 nm excitation. The corresponding component spectra (Figure 2C) are assigned to (i) inter-C_{60} CT excitons characterized by a pronounced EA signal similar to that in neat C_{60} films (Figure S7), (ii) Frenkel excitons showing photoinduced absorption at 550 and 950 nm, and (iii) the charge-induced spectrum consisting of a shifted EA signal together with TAPC$^{\bullet+}$ (~710 nm) and $C_{60}^{\bullet-}$ (~1055 nm) absorption. There is a rapid decay (<1 ps) of the inter-C_{60} CT excitons and concomitant rise of Frenkel excitons, which in turn convert to the charge component on a time scale similar to that with 610 nm excitation. The ultrafast relaxation is absent when Frenkel excitons are directly generated at 610 nm and in the 50% BHJ at both excitation wavelengths (Figure S8), because no C_{60} clusters (and thus no inter-C_{60} CT excitons) are present in the intermixed blend.

We conclude that most of the initially generated inter-C_{60} CT excitons in C_{60} clusters of the dilute blend with 450 nm excitation first undergo ultrafast relaxation to Frenkel excitons before the latter diffuse to TAPC molecules and undergo HT. It has been suggested that direct charge generation via inter-C_{60} CT excitons in neat fullerene domains contributes to photocurrent generation in organic solar cells,[32,33] but our results show that the inter-C_{60} CT excitons do not significantly affect the charge generation mechanism, disproving that bulk-ionization and intermolecular exciton delocalization are relevant for the operation of C_{60}-based dilute-donor systems. The EQE spectrum (Figure 2A, inset) shows photocurrent generation from spectral regions of both inter-C_{60} CT and Frenkel transitions. This is in contrast to neat C_{60} devices, where only inter-C_{60} CT excitons yield photocurrent.[23] The entire Frenkel and CT spectral range of the fullerene absorption can therefore be exploited to generate charges in dilute-donor BHJs.

The EA signatures observed in our systems are a result of a field-induced shift in the ground-state absorption of inter-C_{60} CT transitions in the 400−500 nm region. Upon 450 nm excitation of the 5% TAPC:C_{60} blend, two main sources of electric field can be identified, which both provoke a photoinduced EA response in neighboring C_{60} clusters: first, the short-lived inter-C_{60} CT excitons, and second, the charges formed between the TAPC donor and C_{60} acceptor. In Figure 3A, we compare the TA spectra at an early time delay (0.2 ps), where we have predominantly inter-C_{60} CT excitons, and at 100 ps, where the EA signal is generated by TAPC$^{\bullet+}$/$C_{60}^{\bullet-}$ charges. At 0.2 ps, the oscillatory EA signature corresponds to the steady-state bulk EA signal recorded on a neat C_{60} device under reverse bias (red dotted line), while the EA is clearly blue-shifted at 100 ps (the manually shifted steady-state EA is shown as a dotted blue line to illustrate this). By taking the zero-crossing of the TA spectra, we have time-resolved the gradual shift of the EA (Figure 3B), which occurs within a few picoseconds. EA signatures, and their corresponding spectral positions, have been previously used to probe the energetics of the local environment of charges.[34−36] Therefore, we interpret the shift in EA as a difference in the energetics of the C_{60} clusters. As the EA at early times is caused by inter-C_{60} CT

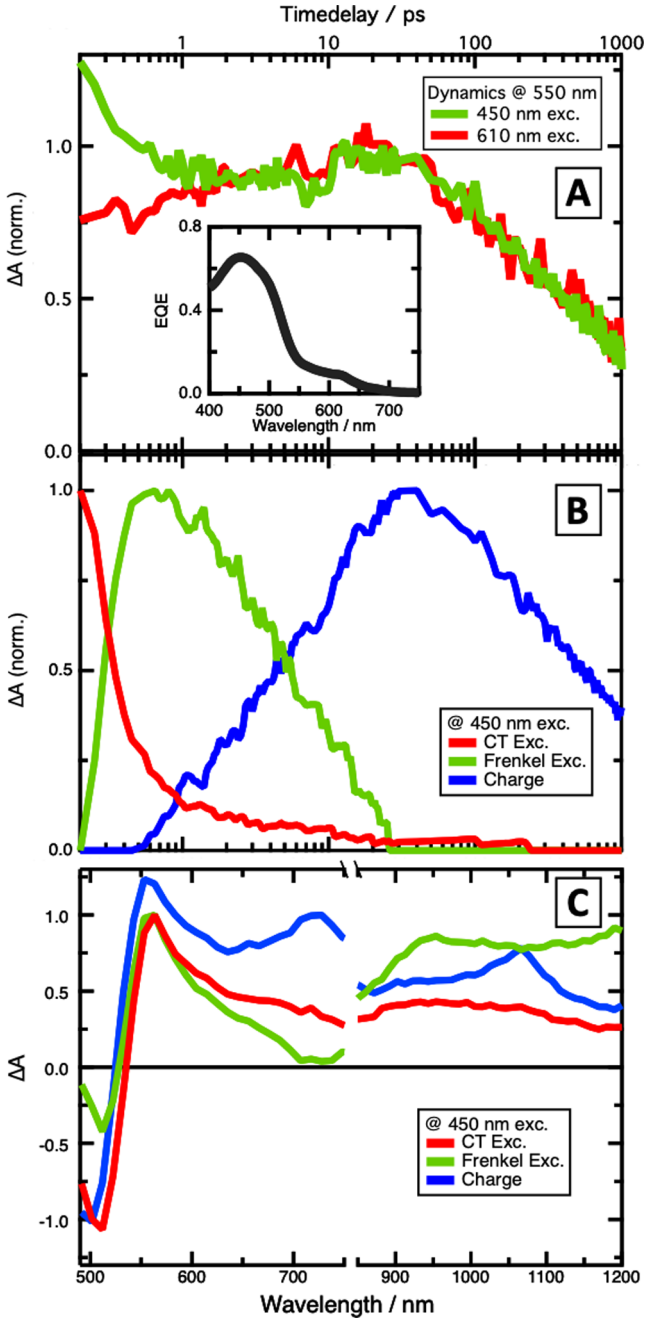

Figure 2. (A) Dynamics of the TA spectra probed at 550 nm (EA peak overlapping with photoinduced absorption) of the 5% TAPC:C_{60} blend excited at 450 nm (green line) and 610 nm (red line, see Figure 1B), normalized to the maximum of the dynamics with 610 nm excitation. The inset shows the EQE spectrum of the dilute 5% TAPC:C_{60} blend. (B) MCR-ALS decomposition of the TA spectra of the 5% TAPC:C_{60} blend excited at 450 nm, with the dynamics of inter-C_{60} CT excitons in red, of Frenkel excitons in green, and of charges in blue. The spectra of those MCR-ALS components are shown in panel C with the same color coding.

https://dx.doi.org/10.1021/acs.jpclett.0c01495
J. Phys. Chem. Lett. 2020, 11, 5610−5617

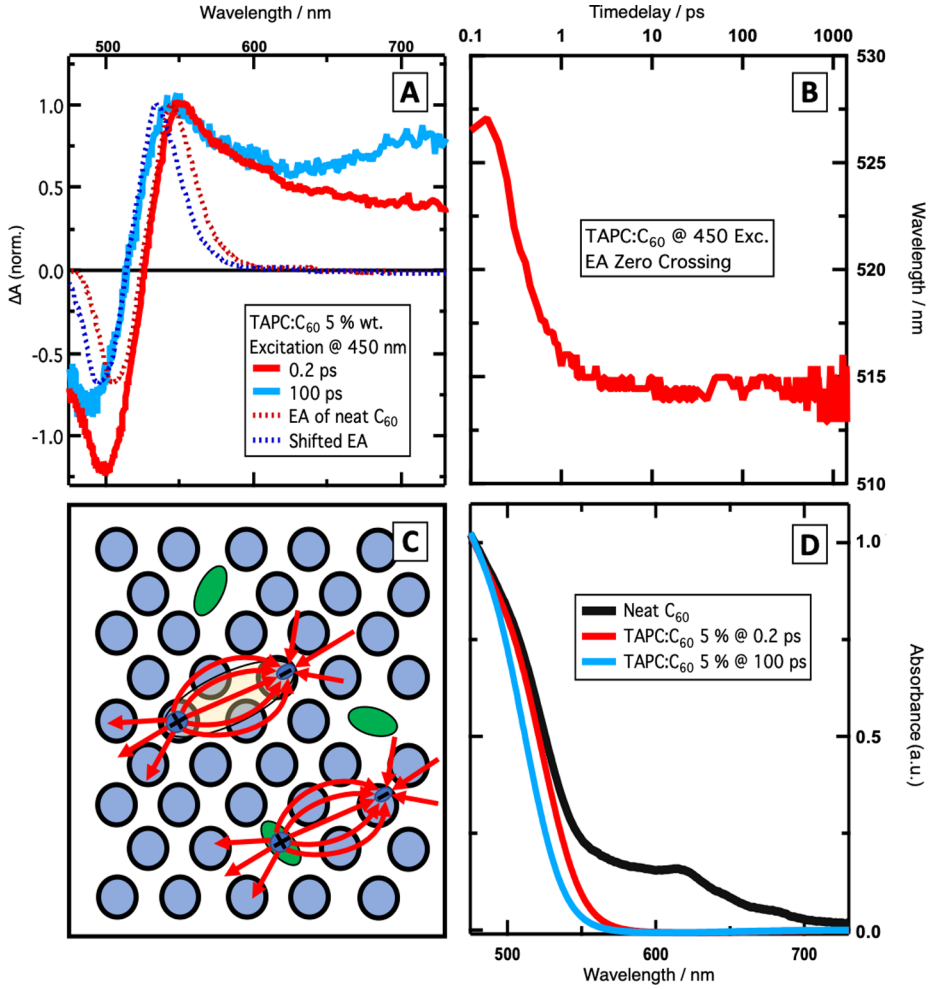

Figure 3. (A) Normalized TA spectra of the 5% TAPC:C_{60} blend excited at 450 nm, at 0.2 ps (solid red) and 100 ps (solid blue), together with the steady-state EA signature recorded in a neat C_{60} device (dotted red line), which is also shown manually shifted to match the zero crossing point at 100 ps (dotted blue line). (B) Time evolution of the zero crossing point of the EA signal from the TA spectra. (C) Schematics of the electric fields responsible for the EA, as produced by inter-C_{60} CT excitons in C_{60} clusters and by charges generated by HT to TAPC molecules. (D) Calculated absorption spectra of C_{60} clusters from double integration of the EA signal at different times (0.2 ps red, 100 ps blue), compared to the absorption spectrum of neat C_{60} film (black).

excitons in bulk C_{60} clusters, we assign the EA position to the local energy environment within these clusters. Then, the later time EA is caused by charges at the TAPC:C_{60} interface (with the holes remaining on TAPC), so that the shifted EA position is assigned to a different local energy environment in C_{60} clusters near the TAPC donors (Figure 3C).

By integrating both the early and late EA signals twice (because the EA in C_{60} has a second derivative line-shape compared to the absorption),[37−39] we are able to reconstruct the absorption spectra of the C_{60} clusters both in the bulk and close to the TAPC donor (Figure 3D). We thus selectively monitor the absorption of interfacial C_{60} clusters, which is not possible with bulk techniques. The calculated absorption spectrum at early times fits well with the steady-state CT absorption of neat C_{60}, because the EA originates from bulk C_{60} clusters. At later times, the calculated absorption spectrum from C_{60} clusters near a TAPC molecule is blue-shifted by 10 nm (or 4.5 meV). The energetic shift between C_{60} clusters near and far from a TAPC donor is likely due to either the disruption of crystallinity in the clusters or to inter-C_{60} interactions between C_{60} and TAPC molecules.[14,40,41] Because C_{60} molecules near TAPC are at higher energy than those in the bulk, an energetic driving force exists that aids electrons to separate from positively charged TAPC molecules after HT and might also hamper the re-encounter of free charges during bimolecular recombination.[40,42] The benefits of such an energetic gradient have been evoked earlier as an important factor promoting free charge generation in organic solar cells,[43−46] together with other parameters such as enhanced charge delocalization into the C_{60} clusters,[35,47,48] high electron mobility,[43] or entropic effects.[49]

Given the presence of neat fullerene regions and the observed energy gradient, we expect that electrons in the dilute TAPC:C_{60} blends efficiently dissociate from holes, allowing ultrafast separation into free charges.[34,47,50−52] This should prevent geminate charge recombination (gCR), a common loss mechanism in intimately mixed systems, where charges cannot escape their mutual attraction and recombine at the donor−acceptor interface.[34,50,53] Nevertheless, monomolecular (fluence-independent) charge recombination is seen in all films on the hundreds of picoseconds time scale (Figure 1C). Surprisingly, this is even more pronounced in the 5% than the 50% BHJ with, respectively, 75% and 42% of charges recombining within 1 ns (Table 1). We suggest that the

https://dx.doi.org/10.1021/acs.jpclett.0c01495
J. Phys. Chem. Lett. 2020, 11, 5610−5617

subnanosecond recombination mechanisms are different in the dilute and intermixed blends. While charges remain mostly bound in interfacial CT states and undergo gCR in the 50% BHJ, CT dissociation is much more efficient in the 5% blend, but the highly mobile free electrons can also readily find trapped holes and reform CT states from where they can undergo monomolecular trap-based recombination.[54] The overall recombination is in both cases rate-limited by CT decay to the ground state, which proceeds with a similar time constant of 280 ps (Table 1), because TAPC:C_{60} CT states are at the same energy independently of the donor concentration.[55] This mechanism is consistent with previous work that has shown that interfacial CT states dissociate faster than they recombine in dilute TAPC:C_{60} blends[8] and with a study modeling the high V_{OC} of ultradilute (<1% donor-content) devices in terms of hole trapping/detrapping at donor sites.[21] Trap-assisted recombination plays a smaller role in the 50% blend, because the electron mobility decreases (disruption of the C_{60} crystallinity at higher TAPC concentration),[7,56] while the hole mobility increases (hole percolation pathways).[18]

In the dilute BHJs, holes move predominantly via long-range tunneling between isolated donor molecules,[18,20] so that their mobility is orders of magnitude lower than that of the electrons in the C_{60} domains, as shown for both the steady-state and relevant <1 ns transient mobilities.[7,18] We can therefore indeed consider the holes to be trapped on isolated TAPC molecules during the investigated time window. To evaluate the effect of reducing the electron mobility in the dilute blends, we show the temperature-dependent TA dynamics at short (<1 ns) and long (<10 μs) time scales for the 5% BHJ in Figure 4A. Supporting the trap-assisted recombination mechanism, when the electron motion is slowed from ~10^0 $cm^2\,V^{-1}\,s^{-1}$ at 300 K to ~10^{-3} $cm^2\,V^{-1}\,s^{-1}$ at 80 K,[57] they encounter fewer trapped holes and the <1 ns recombination is absent. In addition, freezing of exciton diffusion and reduction of the intrinsic rates lead to overall slower dynamics at 80 K.

The lower offset representing long-lived charges in the dilute 5% blend compared to the 50% BHJ (25% versus 58%) shows that the trap-assisted mechanism leads to an even higher fraction of charge loss than gCR (Table 1). This trend contradicts the higher reported PCE and short-circuit current density (2.8%, 5.94 $mA{\cdot}cm^{-2}$) in the dilute compared to the intermixed system (0.3%, 1.45 $mA{\cdot}cm^{-2}$).[7] To resolve this discrepancy, we measured TA spectra on the 5% blend in a full device with a semitransparent back electrode (ITO/MoO_x (2 nm)/5%-TAPC:C_{60} (50 nm)/BPhen (6 nm)/ Al (10 nm)) at V_{OC} (no external circuit). The device was excited at 450 nm to avoid strong scattering of the pump in the TA probe range. The notably faster decay of the C_{60} anion peak at 1050 nm observed in the device compared to the thin film (Figure 4B) supports some electron extraction from the active layer into the Al electrode on the <1 ns time scale. Such fast electron extraction is consistent with previous TREFISH (time-resolved electric-field-induced second harmonic generation) measurements, where electrons were extracted from dilute systems within 20−1000 ps, while hole extraction occurred only after 200 ns.[18] Because electrons are extracted on a time scale relevant to trap-assisted recombination, we suggest that in dilute TAPC devices, the highly mobile electrons rapidly leave the active layer and are thus not able to recombine with trapped holes. We cannot unambiguously confirm slower decay of the hole population in the device, because a large EA signature (caused by additional fields in the device) dominates

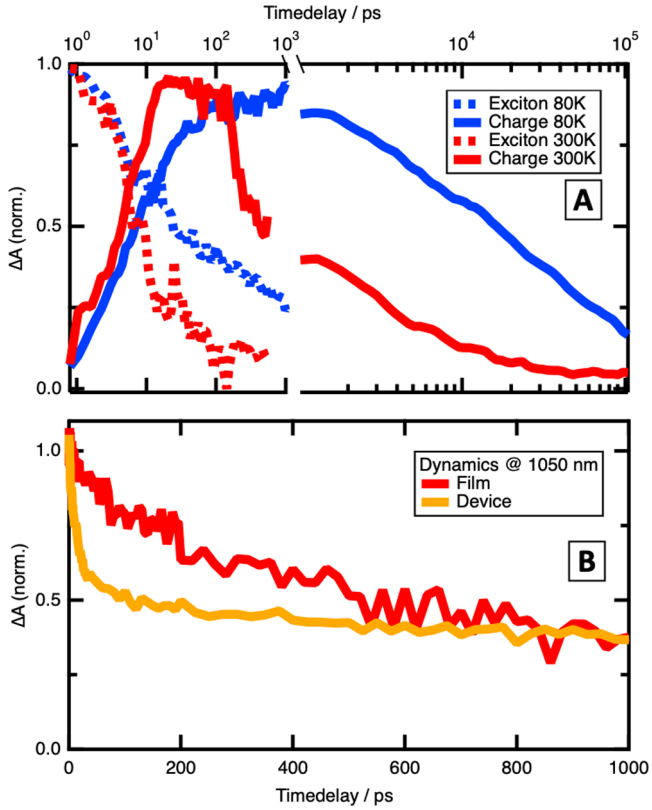

Figure 4. (A) MCR-ALS decomposition dynamics of the exciton (dashed lines) and charge (solid lines) components of a 5% TAPC:C_{60} thin film excited at 532 nm at 80 K (blue lines) and at 300 K (red lines). (B) TA dynamics probed at the C_{60} anion peak (~1050 nm) for a 5% TAPC:C_{60} film without contacts (red) and the corresponding device (orange), both excited at 450 nm.

the visible spectral range of the TA spectrum (Figure S9A). The slower decay of the EA compared to the film could nevertheless indicate that some charges live longer in the device (Figure S9B).

In OPV operating conditions, the faster electron than hole extraction results in a lower electron density in the active layer, suppressing trap-based recombination that we see by TA spectroscopy in the uncontacted films. This contributes to the higher PCE in dilute blends compared to intermixed morphologies, where charges are lost because of gCR even in device configuration. In general, the fast trap-based recombination can harm the performance of dilute solar cells, if charge extraction cannot effectively compete. For C_{60}-based systems containing different dilute donors, this might contribute to the observed strong field dependence, low fill factor, and poor PCE of systems with low-lying interfacial CT states, where the intrinsic recombination rate is enhanced,[8] increasing the recombination probability when a free electron encounters a trapped hole.

In conclusion, we have investigated vapor-deposited organic solar cells based on TAPC:C_{60} blends with low (5% and 10%) and high (50%) donor concentration, creating dilute and molecularly mixed morphologies, respectively. In agreement with previous work on solution-processed solar cells, we find that large C_{60} domains in the dilute blends lead to exciton diffusion-limited hole transfer and assist the generation of free electrons. In addition, we directly visualize, via a gradual shift of the electro-absorption, an energetic gradient driving

https://dx.doi.org/10.1021/acs.jpclett.0c01495
J. Phys. Chem. Lett. 2020, 11, 5610−5617

electrons away from the TAPC site into the C_{60} bulk. We show that charge-transfer excitons within C_{60} clusters (and any related intermolecular delocalization and autoionization) do not play a key role in the hole-transfer process, because they undergo rapid localization to Frenkel excitons before dissociating. The entire Frenkel and charge-transfer range of the fullerene absorption can thus be exploited for charge generation. Finally, we identify a fast monomolecular trap-based recombination mechanism in thin films containing 5% TAPC, where free electrons recombine with holes that are trapped on isolated TAPC molecules. Dilute TAPC:C_{60} devices nevertheless have good solar cell efficiency,[8] because this recombination is suppressed when electrons are rapidly extracted. In contrast, hole transfer in the highly intermixed 50% blend leads to bound electron−hole pairs that geminately recombine, causing poor device performance. Overall, dilute morphologies present an opportunity to promote free charge generation in organic solar cells compared to intermixed blends, but the fast trap-based recombination must be overcome by rapid extraction.

■ ASSOCIATED CONTENT

Supporting Information

The Supporting Information is available free of charge at https://pubs.acs.org/doi/10.1021/acs.jpclett.0c01495.

Experimental details, kinetic modeling, and additional figures as mentioned in the main text (PDF)

■ AUTHOR INFORMATION

Corresponding Author

Natalie Banerji − *Department of Chemistry and Biochemistry, University of Bern, 3012 Bern, Switzerland;* orcid.org/0000-0001-9181-2642; Email: natalie.banerji@dcb.unibe.ch

Authors

Gareth John Moore − *Department of Chemistry and Biochemistry, University of Bern, 3012 Bern, Switzerland*

Martina Causa' − *Department of Chemistry and Biochemistry, University of Bern, 3012 Bern, Switzerland*

Josue F. Martinez Hardigree − *Clarendon Laboratory, Department of Physics, University of Oxford, OX1 3PU Oxford, U.K.;* orcid.org/0000-0001-9439-7173

Safakath Karuthedath − *King Abdullah University of Science and Technology (KAUST), KAUST Solar Center (KSC), Physical Science and Engineering Division (PSE), Thuwal 23955-6900, Kingdom of Saudi Arabia;* orcid.org/0000-0001-7568-2825

Ivan Ramirez − *Clarendon Laboratory, Department of Physics, University of Oxford, OX1 3PU Oxford, U.K.*

Anna Jungbluth − *Clarendon Laboratory, Department of Physics, University of Oxford, OX1 3PU Oxford, U.K.*

Frédéric Laquai − *King Abdullah University of Science and Technology (KAUST), KAUST Solar Center (KSC), Physical Science and Engineering Division (PSE), Thuwal 23955-6900, Kingdom of Saudi Arabia;* orcid.org/0000-0002-5887-6158

Moritz Riede − *Clarendon Laboratory, Department of Physics, University of Oxford, OX1 3PU Oxford, U.K.;* orcid.org/0000-0002-5399-5510

Complete contact information is available at: https://pubs.acs.org/10.1021/acs.jpclett.0c01495

Author Contributions

N.B. and M.R. conceived the project, which was led by N.B. Samples were prepared by I.R., A.J., and J.F.M.H, who also did the GIWAXS measurements. TA experiments were carried out by G.J.M., M.C., and N.B (<1 ns time scale, room temperature) and by S.K. in the group of F.L. (long time scales, low temperature). EQE spectra were recorded by I.R. during a STEM visit to TU Dresden. G.J.M. and N.B. analyzed and interpreted the spectroscopic data and wrote the manuscript with input from all other authors.

Notes

The authors declare no competing financial interest.

Data in Figures 1−4 is made publicly available (BORIS Repository, University of Bern, https://doi.org/10.7892/boris.144885).

■ ACKNOWLEDGMENTS

N.B., G.J.M., and M.C. acknowledge the Swiss National Science Foundation (Grant 200020_184819) and the University of Bern for financial support. J.F.M.H and M.R. acknowledge funding from STFC (Grant ST/L006294/1). M.R. acknowledges funding from EPSRC (Grant EP/L026066/1) and the European Union in FP 7 (Grant 630864). This Letter is based upon work from COST Action StableNextSol MP1307 supported by COST (European Cooperation in Science and Technology), which funded Short Term Scientific Missions (STSMs) of I.R. to TU Dresden and of J.F.M.H. to the group of N.B. I.R. and A.J. acknowledge funding from EPSRC Doctoral Training grant awards, and A.J. acknowledges a Wolfson-Marriott Scholarship from Wolfson College, Oxford. Furthermore, this publication is partially based upon work supported by the King Abdullah University of Science and Technology (KAUST) Office of Sponsored Research (OSR) under Award No. OSR-2018-CARF/CCF-3079. The GIWAXS data was obtained during experiment nt13183-1 at Diamond Lightsource beamline I07. We thank Dr. Koen Vandewal, Dr. Donato Spoltore (both TU Dresden), Prof. Dieter Neher (University of Potsdam), and Prof. Martijn Kemerink (University of Heidelberg) for fruitful discussions.

■ REFERENCES

(1) Hou, J.; Inganäs, O.; Friend, R. H.; Gao, F. Organic solar cells based on non-fullerene acceptors. *Nat. Mater.* **2018**, *17*, 119.

(2) Cui, Y.; Yao, H.; Hong, L.; Zhang, T.; Xu, Y.; Xian, K.; Gao, B.; Qin, J.; Zhang, J.; Wei, Z.; et al. Achieving over 15% efficiency in organic photovoltaic cells via copolymer design. *Adv. Mater.* **2019**, *31*, 1808356.

(3) Fan, B.; Zhang, D.; Li, M.; Zhong, W.; Zeng, Z.; Ying, L.; Huang, F.; Cao, Y. Achieving over 16% efficiency for single-junction organic solar cells. *Sci. China: Chem.* **2019**, *62*, 746.

(4) Cui, Y.; Yao, H.; Zhang, J.; Zhang, T.; Wang, Y.; Hong, L.; Xian, K.; Xu, B.; Zhang, S.; Peng, J.; et al. Over 16% efficiency organic photovoltaic cells enabled by a chlorinated acceptor with increased open-circuit voltages. *Nat. Commun.* **2019**, *10*, 2515.

(5) Liu, Q.; Jiang, Y.; Jin, K.; Qin, J.; Xu, J.; Li, W.; Xiong, J.; Liu, J.; Xiao, Z.; Sun, K. 18% efficiency organic solar cells. *Science Bulletin* **2020**, *65*, 272.

(6) Xiao, X.; Bergemann, K. J.; Zimmerman, J. D.; Lee, K.; Forrest, S. R. Small-molecule planar-mixed heterojunction photovoltaic cells with fullerene-based electron filtering buffers. *Adv. Energy Mater.* **2014**, *4*, 1301557.

(7) Zhang, M.; Wang, H.; Tian, H.; Geng, Y.; Tang, C. W. Bulk heterojunction photovoltaic cells with low donor concentration. *Adv. Mater.* **2011**, *23*, 4960−4.
(8) Collado-Fregoso, E.; Pugliese, S. N.; Wojcik, M.; Benduhn, J.; Bar-Or, E.; Perdigón Toro, L.; Hörmann, U.; Spoltore, D.; Vandewal, K.; Hodgkiss, J. M.; et al. Energy-gap law for photocurrent generation in fullerene-based organic solar cells: The case of low-donor-content blends. *J. Am. Chem. Soc.* **2019**, *141* (6), 2329−2341.
(9) Vandewal, K.; Albrecht, S.; Hoke, E. T.; Graham, K. R.; Widmer, J.; Douglas, J. D.; Schubert, M.; Mateker, W. R.; Bloking, J. T.; Burkhard, G. F.; et al. Efficient charge generation by relaxed charge-transfer states at organic interfaces. *Nat. Mater.* **2014**, *13*, 63−8.
(10) Graham, K. R.; Ndjawa, G. O. N.; Conron, S. M.; Munir, R.; Vandewal, K.; Chen, J. J.; Sweetnam, S. M.; Thompson, M. E.; Salleo, A.; Mcgehee, M. D.; et al. The roles of structural order and intermolecular interactions in determining ionization energies and charge-transfer state energies in organic semiconductors. *Adv. Energy Mater.* **2016**, *6*, 1−9.
(11) Schwarze, M.; Schellhammer, K. S.; Ortstein, K.; Benduhn, J.; Gaul, C.; Hinderhofer, A.; Perdigón Toro, L.; Scholz, R.; Kublitski, J.; Roland, S.; et al. Impact of molecular quadrupole moments on the energy levels at organic heterojunctions. *Nat. Commun.* **2019**, *10* (1), 2466.
(12) Bernardo, B.; Cheyns, D.; Verreet, B.; Schaller, R. D.; Rand, B. P.; Giebink, N. C. Delocalization and dielectric screening of charge transfer states in organic photovoltaic cells. *Nat. Commun.* **2014**, *5*, 3245.
(13) Liu, X.; Ding, K.; Panda, A.; Forrest, S. R. Charge transfer states in dilute donor-acceptor blend organic heterojunctions. *ACS Nano* **2016**, *10*, 7619−7626.
(14) Vandewal, K.; Benduhn, J.; Schellhammer, K. S.; Vangerven, T.; Rückert, J. E.; Piersimoni, F.; Scholz, R.; Zeika, O.; Fan, Y.; Barlow, S.; et al. Absorption tails of donor: C_{60} blends provide insight into thermally activated charge-transfer processes and polaron relaxation. *J. Am. Chem. Soc.* **2017**, *139*, 1699−1704.
(15) Benduhn, J.; Tvingstedt, K.; Piersimoni, F.; Ullbrich, S.; Fan, Y.; Tropiano, M.; McGarry, K. A.; Zeika, O.; Riede, M. K.; Douglas, C. J.; et al. Intrinsic non-radiative voltage losses in fullerene-based organic solar cells. *Nature Energy* **2017**, *2*, 17053.
(16) Tietze, M. L.; Tress, W.; Pfützner, S.; Schünemann, C.; Burtone, L.; Riede, M. K.; Leo, K.; Vandewal, K.; Olthof, S. S.; Schulz, P.; et al. Correlation of open-circuit voltage and energy levels in zinc-phthalocyanine: C_{60} bulk heterojunction solar cells with varied mixing ratio. *Phys. Rev. B: Condens. Matter Mater. Phys.* **2013**, *88*, 085119.
(17) Albes, T.; Xu, L.; Wang, J.; Hsu, J. W. P.; Gagliardi, A. Origin of photocurrent in fullerene-based solar cells. *J. Phys. Chem. C* **2018**, *122* (27), 15140−15148.
(18) Melianas, A.; Pranculis, V.; Spoltore, D.; Benduhn, J.; Inganäs, O.; Gulbinas, V.; Vandewal, K.; Kemerink, M. Charge transport in pure and mixed phases in organic solar cells. *Adv. Energy Mater.* **2017**, *7*, 1700888.
(19) Spoltore, D.; Hofacker, A.; Benduhn, J.; Ullbrich, S.; Nyman, M.; Zeika, O.; Schellhammer, S.; Fan, Y.; Ramirez, I.; Barlow, S.; et al. Hole transport in low-donor-content organic solar cells. *J. Phys. Chem. Lett.* **2018**, *9* (18), 5496−5501.
(20) Lee, T.; Sanzogni, A.; Zhangzhou, N.; Burn, P. L.; Mark, A. E. Morphology of a bulk heterojunction photovoltaic cell with low donor concentration. *ACS Appl. Mater. Interfaces* **2018**, *10* (38), 32413−32419.
(21) Sandberg, O. J.; Zeiske, S.; Zarrabi, N.; Meredith, P.; Armin, A. Charge carrier transport and generation via trap-mediated optical release in organic semiconductor devices. *Phys. Rev. Lett.* **2020**, *124* (12), 128001.
(22) Vandewal, K.; Widmer, J.; Heumueller, T.; Brabec, C. J.; McGehee, M. D.; Leo, K.; Riede, M. K.; Salleo, A. Increased open-circuit voltage of organic solar cells by reduced donor-acceptor interface area. *Adv. Mater.* **2014**, *26*, 3839−3843.
(23) Causa', M.; Ramirez, I.; Martinez Hardigree, J. F.; Riede, M.; Banerji, N. Femtosecond dynamics of photoexcited C_{60} films. *J. Phys. Chem. Lett.* **2018**, *9* (8), 1885−1892.
(24) Yamamoto, S.; Guo, J.; Ohkita, H.; Ito, S. Formation of methanofullerene cation in bulk heterojunction polymer solar cells studied by transient absorption spectroscopy. *Adv. Funct. Mater.* **2008**, *18* (17), 2555−2562.
(25) Chekalin, S. V.; Yartsev, A. P.; Sundström, V. The primary stages of the charge carrier photogeneration in C_{60} films studied by the 100-fs laser pulse pump-probe method. *J. Exp. Theor. Phys.* **2001**, *93* (4), 706−716.
(26) Kaneto, K.; Abe, T.; Takashima, W. Evolution of absorption spectra of C_{60} film in solid electrolyte cell during electrochemical reduction. *Solid State Commun.* **1995**, *96* (5), 259−264.
(27) Gasyna, Z.; Andrews, L.; Schatz, P. N. Near-infrared absorption spectra of fullerene (C_{60}) radical cations and anions prepared simultaneously in solid argon. *J. Phys. Chem.* **1992**, *96* (4), 1525−1527.
(28) Jaumot, J.; Gargallo, R.; de Juan, A.; Tauler, R. A graphical user-friendly interface for mcr-als: A new tool for multivariate curve resolution in matlab. *Chemom. Intell. Lab. Syst.* **2005**, *76* (1), 101−110.
(29) de Juan, A.; Tauler, R. Chemometrics applied to unravel multicomponent processes and mixtures: Revisiting latest trends in multivariate resolution. *Anal. Chim. Acta* **2003**, *500* (1), 195−210.
(30) Amrhein, M.; Srinivasan, B.; Bonvin, D.; Schumacher, M. M. On the rank deficiency and rank augmentation of the spectral measurement matrix. *Chemom. Intell. Lab. Syst.* **1996**, *33* (1), 17−33.
(31) Tauler, R. Multivariate curve resolution applied to second order data. *Chemom. Intell. Lab. Syst.* **1995**, *30* (1), 133−146.
(32) Zou, Y.; Holmes, R. J. The role of exciton ionization processes in bulk heterojunction organic photovoltaic cells. *Adv. Energy Mater.* **2015**, *5* (12), 1500019.
(33) Burkhard, G. F.; Hoke, E. T.; Beiley, Z. M.; McGehee, M. D. Free carrier generation in fullerene acceptors and its effect on polymer photovoltaics. *J. Phys. Chem. C* **2012**, *116* (50), 26674−26678.
(34) Causa', M.; De Jonghe-Risse, J.; Scarongella, M.; Brauer, J. C.; Buchaca-Domingo, E.; Moser, J.-E.; Stingelin, N.; Banerji, N. The fate of electron−hole pairs in polymer:Fullerene blends for organic photovoltaics. *Nat. Commun.* **2016**, *7*, 12556.
(35) Gélinas, S.; Rao, A.; Kumar, A.; Smith, S. L.; Chin, A. W.; Clark, J.; van der Poll, T. S.; Bazan, G. C.; Friend, R. H. Ultrafast long-range charge separation in organic semiconductor photovoltaic diodes. *Science* **2014**, *343* (6170), 512−516.
(36) Jakowetz, A. C.; Böhm, M. L.; Sadhanala, A.; Huettner, S.; Rao, A.; Friend, R. H. Visualising excitations at buried heterojunctions in organic semiconductor blends. *Nat. Mater.* **2017**, *16*, 551.
(37) Kazaoui, S.; Minami, N.; Tanabe, Y.; Byrne, H. J.; Eilmes, A.; Petelenz, P. Comprehensive analysis of intermolecular charge-transfer excited states in C60 and C70 films. *Phys. Rev. B: Condens. Matter Mater. Phys.* **1998**, *58* (15), 7689.
(38) Petelenz, P.; Slawik, M.; Pac, B. Electro-absorption spectrum of buckminsterfullerene—evidence for the existence of charge transfer states. *Synth. Met.* **1994**, *64* (2−3), 335−339.
(39) Jeglinski, S.; Vardeny, Z. V.; Moses, D.; Srdanov, V. I.; Wudl, F. Electroabsorption studies of undoped C_{60} thin films. *Synth. Met.* **1992**, *50* (1−3), 557−563.
(40) Jamieson, F. C.; Domingo, E. B.; McCarthy-Ward, T.; Heeney, M.; Stingelin, N.; Durrant, J. R. Fullerene crystallisation as a key driver of charge separation in polymer/fullerene bulk heterojunction solar cells. *Chemical Science* **2012**, *3* (2), 485−492.
(41) Tsoi, W. C.; Spencer, S. J.; Yang, L.; Ballantyne, A. M.; Nicholson, P. G.; Turnbull, A.; Shard, A. G.; Murphy, C. E.; Bradley, D. D. C.; Nelson, J.; et al. Effect of crystallization on the electronic energy levels and thin film morphology of P3HT:PCBM blends. *Macromolecules* **2011**, *44* (8), 2944−2952.
(42) Marin-Beloqui, J. M.; Fallon, K. J.; Bronstein, H.; Clarke, T. M. Discerning bulk and interfacial polarons in a dual electron donor/acceptor polymer. *J. Phys. Chem. Lett.* **2019**, *10* (13), 3813−3819.

https://dx.doi.org/10.1021/acs.jpclett.0c01495
J. Phys. Chem. Lett. 2020, 11, 5610−5617

(43) Burke, T. M.; McGehee, M. D. How high local charge carrier mobility and an energy cascade in a three-phase bulk heterojunction enable > 90% quantum efficiency. *Adv. Mater.* **2014**, *26* (12), 1923−8.
(44) Izawa, S.; Nakano, K.; Suzuki, K.; Hashimoto, K.; Tajima, K. Dominant effects of first monolayer energetics at donor/acceptor interfaces on organic photovoltaics. *Adv. Mater.* **2015**, *27* (19), 3025−3031.
(45) Nakano, K.; Suzuki, K.; Chen, Y.; Tajima, K. Roles of energy/charge cascades and intermixed layers at donor/acceptor interfaces in organic solar cells. *Sci. Rep.* **2016**, *6*, 29529.
(46) Sweetnam, S.; Graham, K. R.; Ngongang Ndjawa, G. O.; Heumuller, T.; Bartelt, J. A.; Burke, T. M.; Li, W.; You, W.; Amassian, A.; McGehee, M. D. Characterization of the polymer energy landscape in polymer:fullerene bulk heterojunctions with pure and mixed phases. *J. Am. Chem. Soc.* **2014**, *136* (40), 14078−88.
(47) Bittner, E. R.; Silva, C. Noise-induced quantum coherence drives photo-carrier generation dynamics at polymeric semiconductor heterojunctions. *Nat. Commun.* **2014**, *5*, 3119.
(48) Jakowetz, A. C.; Böhm, M. L.; Zhang, J.; Sadhanala, A.; Huettner, S.; Bakulin, A. A.; Rao, A.; Friend, R. H. What controls the rate of ultrafast charge transfer and charge separation efficiency in organic photovoltaic blends. *J. Am. Chem. Soc.* **2016**, *138* (36), 11672−11679.
(49) Hood, S. N.; Kassal, I. Entropy and disorder enable charge separation in organic solar cells. *J. Phys. Chem. Lett.* **2016**, *7* (22), 4495−4500.
(50) Scarongella, M.; De Jonghe-Risse, J.; Buchaca-Domingo, E.; Causa', M.; Fei, Z.; Heeney, M.; Moser, J. E.; Stingelin, N.; Banerji, N. A close look at charge generation in polymer:Fullerene blends with microstructure control. *J. Am. Chem. Soc.* **2015**, *137* (8), 2908−18.
(51) Gélinas, S.; Rao, A.; Kumar, A.; Smith, S. L.; Chin, A. W.; Clark, J.; van der Poll, T. S.; Bazan, G. C.; Friend, R. H. Ultrafast long-range charge separation in organic semiconductor photovoltaic diodes. *Science* **2014**, *343* (6170), 512.
(52) Provencher, F.; Bérubé, N.; Parker, A. W.; Greetham, G. M.; Towrie, M.; Hellmann, C.; Côté, M.; Stingelin, N.; Silva, C.; Hayes, S. C. Direct observation of ultrafast long-range charge separation at polymer−fullerene heterojunctions. *Nat. Commun.* **2014**, *5* (1), 4288.
(53) Howard, I. A.; Mauer, R.; Meister, M.; Laquai, F. Effect of morphology on ultrafast free carrier generation in polythiophene: Fullerene organic solar cells. *J. Am. Chem. Soc.* **2010**, *132* (42), 14866−14876.
(54) Street, R. A.; Schoendorf, M.; Lee, J. Y.; Roy, A. Interface state recombination in organic solar cells. *Phys. Rev. B: Condens. Matter Mater. Phys.* **2010**, *81* (20), 205307.
(55) Vandewal, K.; Benduhn, J.; Schellhammer, K. S.; Vangerven, T.; Rückert, J. E.; Piersimoni, F.; Scholz, R.; Zeika, O.; Fan, Y.; Barlow, S.; et al. Absorption tails of donor: C_{60} blends provide insight into thermally activated charge-transfer processes and polaron relaxation. *J. Am. Chem. Soc.* **2017**, *139* (4), 1699−1704.
(56) Pandey, R.; Gunawan, A. A.; Mkhoyan, K. A.; Holmes, R. J. Efficient organic photovoltaic cells based on nanocrystalline mixtures of boron subphthalocyanine chloride and C_{60}. *Adv. Funct. Mater.* **2012**, *22* (3), 617−624.
(57) Singh, T. B.; Marjanović, N.; Matt, G. J.; Günes, S.; Sariciftci, N. S.; Montaigne Ramil, A.; Andreev, A.; Sitter, H.; Schwödiauer, R.; Bauer, S. High-mobility n-channel organic field-effect transistors based on epitaxially grown C_{60} films. *Org. Electron.* **2005**, *6* (3), 105−110.

https://dx.doi.org/10.1021/acs.jpclett.0c01495
J. Phys. Chem. Lett. 2020, 11, 5610−5617